A novel Ni-CERMET electrode based on a proton conducting electrolyte

L. N. VAN RIJ
Laboratory for Inorganic Chemistry, Delft University of Technology, Julianalaan 136, 2628 BL, Delft, The Netherlands
E-mail: L.N.vanRij@tnw.tudelft.nl

J. LE*
Department of Inorganic Materials, East China University of Science and Technology, Shanghai 200237, People's Republic China

R. C. VAN LANDSCHOOT, J. SCHOONMAN
Laboratory for Inorganic Chemistry, Delft University of Technology, Julianalaan 136, 2628 BL, Delft, The Netherlands

Based on the one-chamber fuel cell design by Iwahara a catalytic methane sensor has been developed. The working principle of this sensor is based on the difference in catalytic properties of two electrodes for the CO_2 reforming reaction of methane. The sensor is based on a high-temperature proton conducting electrolyte, i.e. $SrCe_{0.95}Yb_{0.05}O_{3-\alpha}$ or $CaZr_{0.9}In_{0.1}O_{3-\alpha}$. At 500 °C a linear sensor response on the methane partial pressure has been found for a Ru/$SrCe_{0.95}Yb_{0.05}O_{3-\alpha}$/Pt cell. This cell, however, shows poor long-term stability. The long-term stability of the Ru/$SrCe_{0.95}Yb_{0.05}O_{3-\alpha}$/Pt cell is improved using a more stable electrolyte material, i.e. $CaZr_{0.9}In_{0.1}O_{3-\alpha}$(CZI10). Further improvement of the long-term stability of the sensor is achieved using a nickel-$CaZr_{0.9}In_{0.1}O_{3-\alpha}$ CERMET (Ni-CZI10) electrode. The sensor response of a Ni-CZI10/$CaZr_{0.9}In_{0.1}O_{3-\alpha}$/Pt cell is found to be linear at 600 °C and 700 °C, respectively. The temperature dependence of both the Ru/$SrCe_{0.95}Yb_{0.05}O_{3-\alpha}$/Pt and the Ni-CZI10/$CaZr_{0.9}In_{0.1}O_{3-\alpha}$/Pt cell can be explained by the temperature dependence of the catalytic activity of the electrode materials used. This confirms that the obtained EMF is established by a catalytic activity difference between both electrodes. The power output of a Ni-CZI10/$CaZr_{0.9}In_{0.1}O_{3-\alpha}$/Pt cell is also determined. A combined sensor-fuel cell would have the advantage that it is able to detect the fuel concentration in the gas and, therefore, correct *in-situ* for fluctuations in the fuel concentration. The power output of the Ni-CZI10/$CaZr_{0.9}In_{0.1}O_{3-\alpha}$/Pt cell, however, is found to be 0.01 $mW \cdot cm^{-2}$. This low power output, with respect to values reported in literature for the one-chamber fuel cell, can be explained by the relatively thick electrolyte used, the electrode materials chosen, and the use of the reforming reaction of methane instead of the partial oxidation of methane. However, the feasibility of the combined sensor-fuel cell has been demonstrated. © *2001 Kluwer Academic Publishers*

1. Introduction

In the early nineties Iwahara and Hibino have shown the possibility of a fuel cell system that operates on a uniform gas mixture of methane and air [1, 2]. Although the fuel cell system did not produce a sufficient power density (2.36 $mW \cdot cm^{-2}$) to be used for generating electrical power, the system offered the possibility to simplify the fuel cell design enormously. In later years, Iwahara and Hibino were able to steadily increase the power output of this one-chamber fuel cell system to 170 $mW \cdot cm^{-2}$ in 1995 [3, 4]. State-of-the-art one-chamber fuel cells still do not generate more than about 200 $mW \cdot cm^{-2}$ [5–7].

Iwahara *et al*. have shown that the working principle of the one-chamber fuel cell is the difference in catalytic activity of the two electrodes used [1, 2]. Later, Riess *et al*. demonstrated theoretically that a measurable EMF is obtained if there is a selectivity difference between two electrodes [8]. Recently, Jak *et al*. have studied the catalytic properties of electrodes in one-chamber fuel cell systems. They show that in an electrochemical device with two different electrodes the polarity of an electrode depends on both the counter electrode used and the fuel/oxygen ratio in the gas mixture [9]. This confirms that the working principle of these systems is indeed based on the different catalytic properties of the employed electrodes.

The different catalytic properties of two materials also lead to a different methane partial pressure *dependence* of a device using two different electrodes.

Hence, with changing methane partial pressures a different EMF is observed. Based on this partial pressure dependence a methane sensor has been developed in our laboratory, the catalytic asymmetrical methane sensor [10–12]. It has also been shown that for this sensor system the catalytic properties of the electrodes determine the sensor response [10]. There is, however, one important difference between the catalytic asymmetrical methane sensor and the one-chamber fuel cell, i.e. in the one-chamber fuel cell it is necessary to have a catalytic activity difference that is as large as possible in order to obtain a maximal power output. Hence, the counter electrode can even be catalytically inactive. In the sensor application, however, the counter electrode should exhibit at least *some* catalytic activity in order to establish a potential difference that is partial pressure dependent. Furthermore, a catalytic activity difference that is too large leads to non-linearities, as will be shown in this article.

The detection principle of the catalytic asymmetrical methane sensor is based on the difference in catalytic activity of two electrodes for the CO_2-reforming reaction of methane (1). Via this reforming reaction methane is converted into hydrogen and carbon monoxide [13–15].

$$CH_4 + CO_2 \longleftrightarrow 2H_2 + 2CO \qquad (1)$$

Since the catalytic activity of both electrodes is different, a different hydrogen partial pressure will be established at both electrodes. This hydrogen partial pressure difference creates a potential difference across the cell which is a measure of the methane concentration (Fig. 1).

The sensor is based on a proton conducting electrolyte, which is chosen to be either $SrCe_{0.95}Yb_{0.05}O_{3-\alpha}$ (SCYb5) or $CaZr_{0.9}In_{0.1}O_{3-\alpha}$ (CZI10). These materials belong to the class of high-temperature perovskite-type proton conductors and were first discovered by Iwahara *et al*. [16–18]. The materials exhibit proton conduction in the presence of water vapour or hydrogen. The proton is incorporated into the lattice to form a hydroxyl group according to reaction (2) [19–21]

$$H_2O(g) + V_O^{\bullet\bullet} + O_O^x \longrightarrow 2OH_O^{\bullet} \qquad (2)$$

The oxygen vacancies are created as charge compensation during the doping of the perovskite material

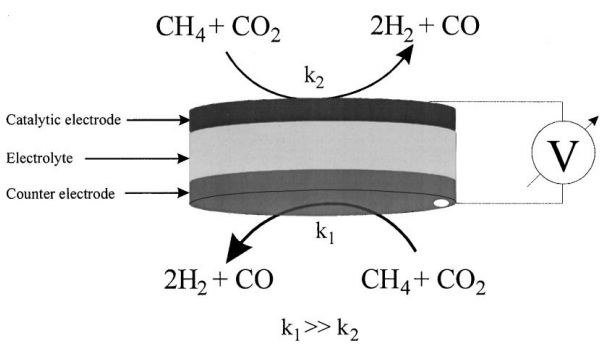

Figure 1 Schematic representation of the catalytic asymmetrical methane sensor.

(ABO_3) with trivalent dopants, like e.g. ytterbium (3):

$$Yb_2O_3 \xrightarrow{ABO_3} 2V''_{Sr} + Yb'_B + 3O_O^x + 3V_O^{\bullet\bullet} \qquad (3)$$

Due to the high protonic conduction of SCYb5, this material has found application in various electrochemical devices, i.e. fuel cells [22, 23], hydrogen pumps [24, 25], (de)hydrogenation reactors [26], and hydrogen sensors [27, 28]. The proton conductivity of zirconates has been found to be lower than the proton conductivity of cerates [29–31]. In-doped $CaZrO_3$, however, still shows appreciable proton conductivity [32, 33]. The main advantage of using $CaZrO_3$ is the high chemical and thermal stability of this material [34] with respect to doped $ACeO_3$ (A=Ba, Sr) [34–36]. Due to this high stability, $CaZrO_3$ is a promising candidate as a solid electrolyte in solid oxide fuel cells and gas sensors [37–39].

2. Experimental aspects

The electrolyte, $SrCe_{0.95}Yb_{0.05}O_{3-\alpha}$ (SCYb5), was synthesised according to the method described by Iwahara *et al*. [40, 41]. A calculated mixture of $SrCO_3$ (Fluka Chemica, >98%), CeO_2 (Fluka Chemica, >99%), and Y_2O_3 (Fluka Chemica, 99.9%) was prepared. After milling in acetone, this mixture was calcined at 1400 °C for 10 hours in air at a heating rate of 5 °C · min^{-1}.

The preparation of $CaZrO_3$ powders, doped with 10 mol % of In_2O_3 (CZI10), has been reported in detail earlier [42, 43]. The starting materials were indium oxide (99.999% In_2O_3, Aldrich Chem. Co.), calcium carbonate (Merck, >99%), and zirconium oxychloride octahydrate (GR, >99% $ZrOCl_2 \cdot 8H_2O$, E. Merck, Germany). Di-ammonium oxalate monohydrate (GR, 99.5–101.0% $(NH_4)_2C_2O_4 \cdot H_2O$, E. Merck, Germany) was used as complexing agent. Polyethyleneglycol 200 (Merck, pro analyse) was added to the precursor solution as a surfactant (5 wt.%). The solution of Ca^{2+}, In^{3+}, and Zr^{4+} [0.1 mol · l^{-1}] was added dropwise to a dilute alkaline $(NH_4)_2C_2O_4 \cdot H_2O$ (Merck, >99%) solution [0.3 mol · l^{-1}] under constant stirring. To ensure complete complexation an excess of 25 wt.% $(NH_4)_2C_2O_4 \cdot H_2O$ relative to the total concentration of cations in the precursor solution was used. The complexation was achieved at 45 ± 2 °C and a pH of 9.0 ± 0.05, which was controlled by continuously adding a concentrated NH_4OH solution. The resulting precipitated complex was calcined at 1450 °C in air using a platinum crucible.

The obtained perovskite powders were milled and shaped into pellets with a diameter of 13 mm and a thickness of about 1 mm using cold uniaxial pressing. Before pressing the powders a binder (Hoechst wachs C micro binder) was added to the mixture. Finally, the pellets were sintered in air at 1400 °C for 10 hours (SCYb5) or 1550 °C/10 hours (CZI10). In both cases the heating rate used was 5 °C · min^{-1}.

In the cell based on SCYb5 ruthenium was chosen as the catalytic electrode, because of the high catalytic activity for the CO_2-reforming of methane [13, 15].

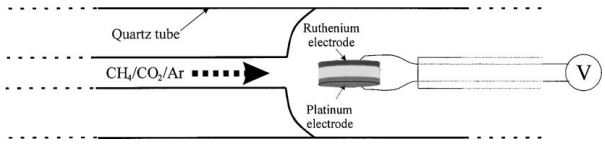

Figure 2 Schematic representation of the one compartment set-up used.

This metal electrode was deposited using a vacuum-evaporation unit. A tungsten crucible was filled with 2 mg of ruthenium, and a current of 85 A was applied to the crucible for 30 s. The pressure was kept at 3×10^{-8} bar.

As counter electrode platinum was used in this cell. This electrode was deposited using a sputter coater (Edwards Sputter Coater S150B). The electrode was sputtered in an argon atmosphere for 1.5 min at a pressure of 7 mbar, a voltage of 1 kV, and a current of 20 mA. To obtain a stable electrode it is necessary to repeat this deposition process four times, with a intermediate heat treatment after each deposition at 800 °C for 10 hours in air.

When CZI10 was used as electrolyte material nickel was chosen as catalytic electrode. To obtain a stable electrode a nickel-CZI10 CERMET was developed. The Ni-CZI10 porous cermet film has been prepared by making a paste using Ni-metal powder, the synthesised CZI10 electrolyte, and a polymer binder (PVC) to which tetrahydrofuran (THF) was added as a solvent. This paste was applied to one surface of the electrolyte pellet using spin coating. The applied CERMET was subsequently sintered in argon at 1100 °C. As counter electrode Pt paste was painted on the $CaZr_{0.9}In_{0.1}O_{3-\alpha}$ electrolyte. After drying at room temperature, a porous conducting Pt film was formed.

Scanning Electron Microscope (SEM) images of the electrolyte and the nickel CERMET were taken using a Jeol LV 5800 scanning electron microscope.

The sensor activity was tested in a single-compartment set-up as depicted in Fig. 2. The experiments were performed at temperatures of 500 °C, 600 °C, and 700 °C, respectively, in $CH_4/CO_2/Ar$ mixtures. The methane concentration was varied between 1.5 and 80 vol.%, while the CO_2 concentration was 5, 10, 20, or 40 vol.%. The gas flow rate was 25 ml · min^{-1} in all experiments.

3. Results and discussion

3.1. Sensor characteristics of the $Ru/SrCe_{0.95}Yb_{0.05}O_{3-\alpha}/Pt$ cell

The sensor response of a $Ru/SrCe_{0.95}Yb_{0.05}O_{3-\alpha}/Pt$ cell as a function of the applied methane partial pressure at different temperatures is shown in Fig. 3. The effect of temperature on the sensor response is not straightforward. With increasing temperature the catalytic activity of the electrodes for the CO_2-reforming of methane, increases. An increase in the catalytic activity leads to a higher hydrogen production and can, therefore, lead to a higher EMF. This higher EMF will only be established if the catalytic electrode shows a larger increase in catalytic activity than the counter electrode used. If the counter electrode shows a larger temperature dependence, the opposite is observed and, hence, the measured EMF is lower. Furthermore, an increase in temperature leads to an increase in the EMF, according to Nernst law. As can be seen, at 500 °C a linear sensor response is obtained. At 450 °C, however, an exponential behaviour is found. At temperatures higher than 500 °C, the sensor response levels off, especially at methane concentrations higher than 5 vol.%. At 650 °C a linear response curve is found again, but the sensitivity of the sensor at this temperature is much lower than at 500 °C. The explanation for this behaviour can be found in the temperature dependence of the catalytic activity of the used ruthenium and platinum electrodes. The exponential behaviour at 450 °C can be attributed to a low catalytic activity of the counter electrode. At low methane partial pressures the catalytic activity of both metals is small and this leads to a small EMF. When the partial pressure of methane is increased the most sensitive electrode, i.e. the catalytic electrode, starts to catalyse the reforming of methane to hydrogen and an increase in the EMF is observed. This increase is not linear, because the catalytic activity of the counter electrode is still very small and this electrode is not very sensitive to concentration differences at this temperature [13].

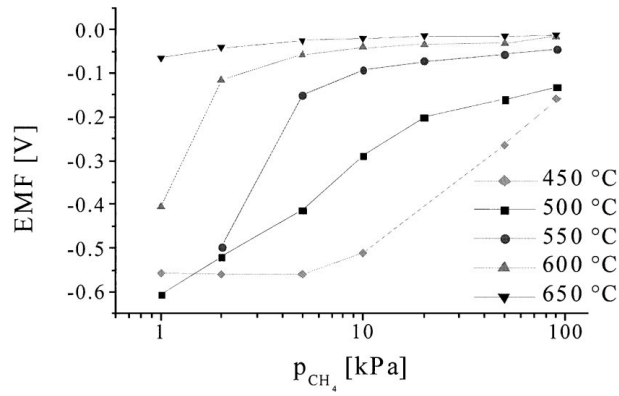

Figure 3 The measured temperature dependence of a $Ru/SrCe_{0.95}Yb_{0.05}O_{3-\alpha}/Pt$ cell in 5 vol.% CO_2.

At a temperature of 500 °C, both electrodes show some catalytic activity towards the CO_2-reforming of methane [13]. A linear dependence on the methane partial pressure can only be found, if the influence of the methane partial pressure on the conversion efficiency of both metals is similar. In other words, the response of platinum and ruthenium to *changes* in the methane concentration is the same, only the reaction rate at a *given* methane partial pressure is higher at the Ni-electrode. This result shows that the choice of the counter electrode is as important as the catalytic electrode. Both electrodes should exhibit a catalytic activity that is high enough to establish a hydrogen partial pressure. However, if the difference in catalytic properties between the electrodes is too high, the sensor response will not be linear. If, on the other hand, the difference in catalytic activity is too small, the sensitivity of the sensor will be poor. In the case of a fully inert counter electrode a potential difference will not be established at all, since there is no hydrogen partial pressure difference created. The effect of a small catalytic activity

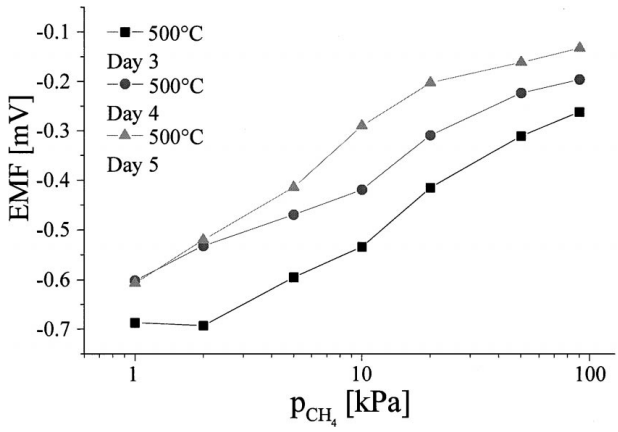

Figure 4 The sensor reponse of a Ru/$SrCe_{0.95}Yb_{0.05}O_{3-\alpha}$/Pt cell measured at 500 °C and 5 vol.% CO_2 for three consecutive days.

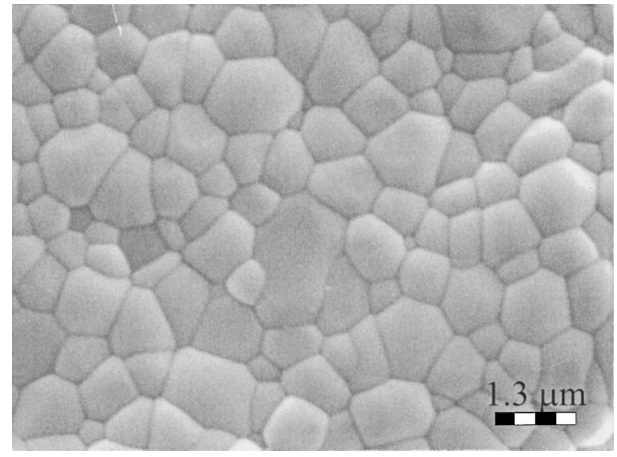

Figure 6 SEM image of the surface of a $CaZr_{0.9}In_{0.1}O_{3-\alpha}$ (CZI10) pellet.

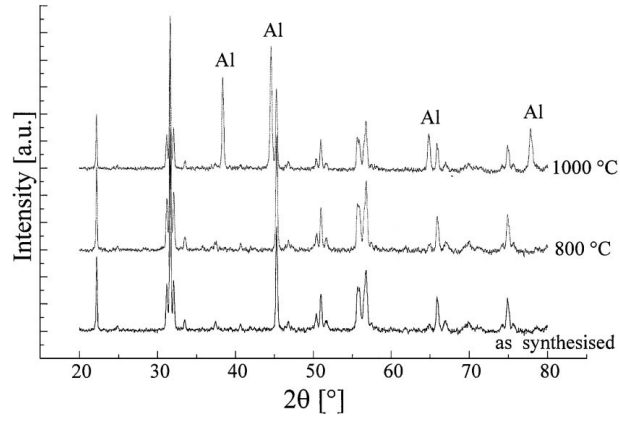

Figure 7 XRD patterns of $CaZr_{0.9}In_{0.1}O_{3-\alpha}$ as synthesised and after testing in 10 vol.% CO_2 and 10 vol.% CH_4 at 800 °C and 1000 °C, respectively. All unlabeled peaks are attributed to $CaZr_{0.9}In_{0.1}O_{3-\alpha}$. The peaks labelled "Al" are due to the aluminium sample holder.

difference is found at 650 °C. The catalytic activity of Pt for the CO_2-reforming of methane increases steeper with temperature than the activity of Ru [13]. In other words, with increasing temperature the catalytic activity difference between Ru and Pt becomes smaller. This implies that the sensitivity of the sensor will decrease with temperature, as measured at 650 °C.

Fig. 4 shows the stability of the catalytic asymmetrical methane sensor using $SrCe_{0.95}Yb_{0.05}O_{3-\alpha}$ (SCYb5) as electrolyte. It is evident that the stability of this sensor system is very poor. Although the sensitivity of the sensor system is comparable on each day, the absolute value of the measured EMF at one methane partial pressure changes within one day, which is, of course, not desirable.

3.2. Chemical stability $SrCe_{0.95}Yb_{0.05}O_{3-\alpha}$ and $CaZr_{0.9}In_{0.1}O_{3-\alpha}$

The poor long-term stability of the Ru/$SrCe_{0.95}Yb_{0.05}O_{3-\alpha}$/Pt sensor (Fig. 4) is caused by the chemical instability of the employed electrolyte in CO_2 and CH_4 containing ambients. Fig. 5 shows the XRD patterns of SCYb5 after placing this material for ca. 100 hours in 10 vol.% CO_2 and 10 vol.% CH_4 at 800 °C and 1000 °C, respectively. For reference the XRD pattern of the material as synthesised is also presented. Rare-earth doped cerates are reported to be thermodynamically unstable in CO_2 containing ambients [34, 36]. The results presented in Fig. 5 confirm this. If SCYb5 is placed in an ambient containing 10 vol.% CO_2 and 10 vol.% CH_4, the material reacts to form $SrCO_3$, CeO_2, and YbOOH. This reaction is quite fast, within four days the electrolyte decomposes to form the products mentioned.

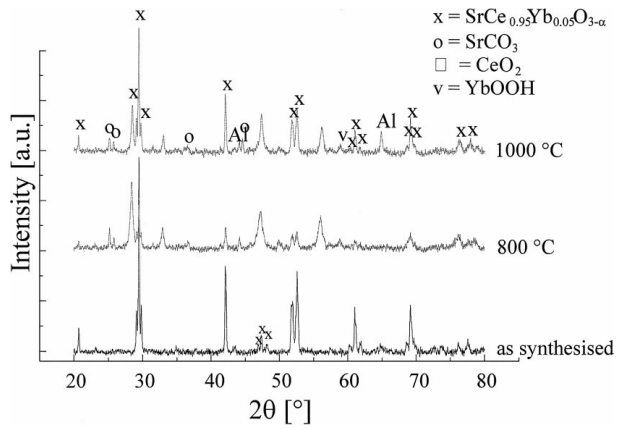

Figure 5 XRD patterns of $SrCe_{0.95}Yb_{0.05}O_{3-\alpha}$ as synthesised and after testing in 10 vol.% CO_2 and 10 vol.% CH_4 at 800 °C and 1000 °C, respectively. The peaks labelled "Al" are due to the aluminium sample holder.

To be able to construct a methane sensor that has a good long-term stability another electrolyte material needs to be used. Therefore, SCYb5 is replaced with $CaZr_{0.9}In_{0.1}O_{3-\alpha}$ (CZI10). This material is known to be more stable than SCYb5, both chemically and thermally [34]. The CZI10 material is synthesised wet-chemically using a peroxo-oxalate complexation method. A SEM image of the surface of a CZI10 pellet is given in Fig. 6. The stability of the CZI10 material is tested in the same way as that of SCYb5, i.e. placing the material for about 100 hours in 10 vol.% CO_2 and 10 vol.% CH_4 at 800 °C and 1000 °C. The XRD patterns of the material after testing and as synthesised are represented in Fig. 7. It can easily be seen that this material does not decompose, as does SCYb5. It is, therefore, assumed that the application of this material as the electrolyte in the catalytic asymmetrical methane sensor will result in a more stable response.

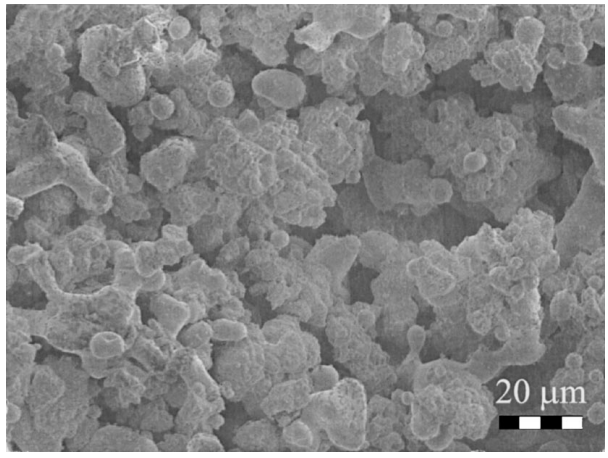

(A)

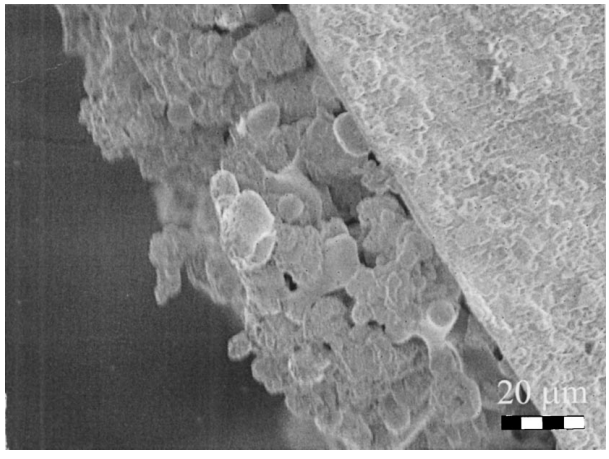

(B)

Figure 8 SEM images of: A) Surface of the nickel-CZI10 CERMET B) Cross-section of the nickel-CZI10 CERMET in contact with $CaZr_{0.9}In_{0.1}O_{3-\alpha}$.

3.3. Nickel-$CaZr_{0.9}In_{0.1}O_{3-\alpha}$ CERMET electrode

To further increase the long-term stability of the sensor system a nickel-CZI10 CERMET has been developed. Fig. 8a and b show a SEM image of the surface and cross-section of this CERMET. As can be seen in the SEM images, the CERMET film is highly porous. There is a continuous network of both the nickel and the CZI10 particles, resulting in a high electronic conductivity of the film. The porous structure also ensures a large gas/electrode/electrolyte three-phase boundary (tpb) and hence an adequate methane conversion. Furthermore, the use of a CERMET electrode prevents the dispersed Ni particles from sintering during high-temperature operation. Hence, a good long-term stability of the electrode is expected, which will also improve the reproducibility of the sensor. The large three-phase boundary facilitates the electrolyte/electrode interface reaction with hydrogen in order to establish a potential. As a result of both the enhanced conversion and interfacial reaction efficiency, the sensitivity of the sensor is also increased. In other words, the application of the nickel-CERMET results in a higher stability and an improved sensitivity of the sensor. The Ni-CZI10 CERMET exhibits excellent adhesion and thermal stability, as well as a good electrical conductivity. In a reducing atmosphere of 5 vol.% H_2 in argon, the CERMET film is stable up to eight thermal cycles from room temperature up to 800 °C [10]. After these cycles both the adhesion and the electrical conductivity of the film have not markedly changed.

3.4. Sensor characteristics of the Ni-CZI10/$CaZr_{0.9}In_{0.1}O_{3-\alpha}$/Pt cell

Fig. 9 shows the sensor response of a Ni-CZI10/$CaZr_{0.9}In_{0.1}O_{3-\alpha}$/Pt sensor in a gas mixture of methane with 5 vol.% CO_2 and Ar gas at 500 °C, 600 °C, and 700 °C, respectively. At each temperature a clear increase in the measured EMF with increasing methane partial pressure is observed. This methane partial pressure dependence shows the possibility of the Ni-CZI10/CZI10/Pt sensor to detect methane in the absence of oxygen as shown above for the Ru/$SrCe_{0.95}Yb_{0.05}O_{3-\alpha}$/Pt cell. At 600 °C and 700 °C a linear sensor response is observed with a sensitivity of 56 [mV/decade] and 26 [mV/decade], respectively, while at a temperature of 500 °C the sensor response is exponential. This temperature dependence is analogous to the temperature dependence of the Ru/SCYb5/Pt cell. At 500 °C the counter electrode, platinum, has a low catalytic activity [13,15]. Therefore, the EMF changes are caused by changes in the catalytic activity of the ruthenium electrode. Because the activity of this electrode does not change linearly with increasing methane partial pressure, a non-linear sensor response is observed. At 600 °C the activity of the platinum electrode has increased [13,15] and both electrodes now change their activity with increasing methane partial pressure, resulting in a linear behaviour of the sensor. At 700 °C the activity difference between the electrodes has decreased, due to the higher temperature dependence of the activity of the platinum electrode [13]. A lower difference in catalytic activity leads to a lower sensitivity of the sensor as observed at 700 °C.

Because the sensor principle is based on the CO_2-reforming reaction of methane the catalytic methane sensor has an intrinsic CO_2 dependence. Just as an increase in the methane partial pressure influences the EMF via reaction (1), an increase in the CO_2 concentration will also result in an EMF change.

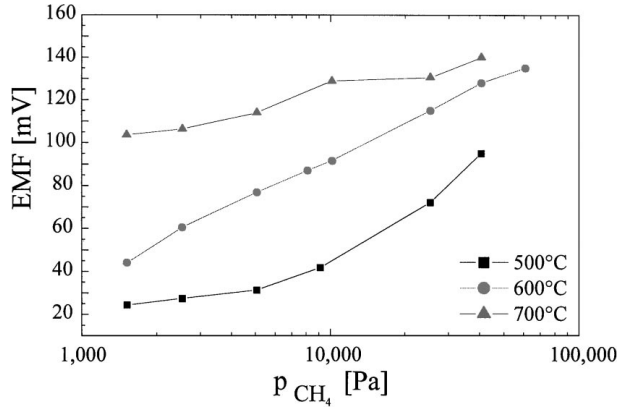

Figure 9 The measured temperature dependence of a Ni-CZI10/$CaZr_{0.9}In_{0.1}O_{3-\alpha}$/Pt cell in 5 vol.% CO_2.

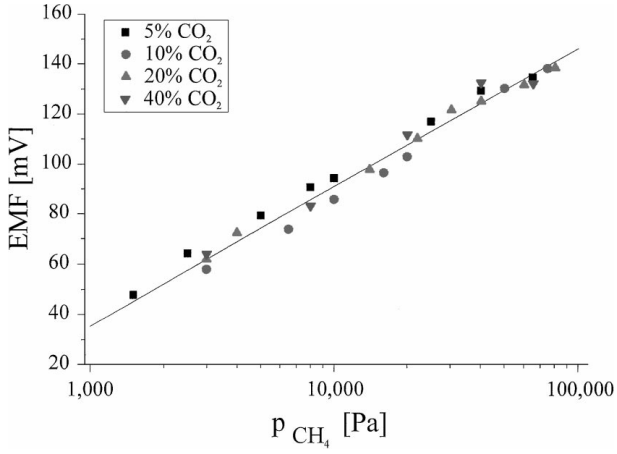

Figure 10 The sensor response at 600 °C of a Ni-CZI10/$CaZr_{0.9}In_{0.1}O_{3-\alpha}$/Pt cell at different CO_2 concentrations. The measured EMF is corrected to a CO_2 concentration of 0 vol.%.

Indeed, the sensor reponse has been found to depend on the CO_2 concentration. Fortunately, this CO_2 dependence is linear. Therefore, it is easy to extrapolate the measured EMF to a CO_2 concentration of 0 vol.%. This extrapolated EMF is now independent of the CO_2 concentration. The response curve, after this correction has been made, is shown in Fig. 10. Although the empirical correction leads to a uniform and CO_2 independent response curve a more fundamental equation is necessary in order to obtain a more detailed understanding of the sensing principle. The empirical correction is, however, extremely useful to show the possibility to apply the sensor in an atmosphere with a fluctuating CO_2 partial pressure.

The stability and reproducibility of the Ni-CZI10/CZI10/Pt sensor system in a gas atmosphere with 10 vol.% CO_2 at 600 °C is shown in Fig. 11. As can be seen, the sensor response is very reproducible, i.e. after 960 hours of operation the same EMF is measured as after working for 480 hours. The increased long-term stability of the sensor is attributed to both the stability of the CERMET electrode and the high chemical stability of the $CaZr_{0.9}In_{0.1}O_{3-\alpha}$ electrolyte in CO_2-containing atmospheres as discussed above.

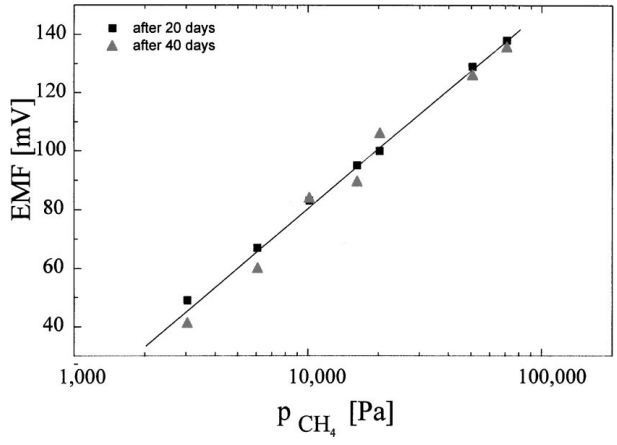

Figure 11 The sensor response of a Ni-CZI10/$CaZr_{0.9}In_{0.1}O_{3-\alpha}$/Pt cell at 500 °C and 10 vol.% CO_2 after 20 and 40 days, respectively.

3.5. Combined fuel cell sensor characteristics of the Ni-CZI10/$CaZr_{0.9}In_{0.1}O_{3-\alpha}$/Pt cell

As discussed in the introduction, the catalytic methane sensor is based on the one-chamber fuel cell design by Iwahara *et al.* [1, 2]. Therefore, it should be possible to construct an electrochemical device that combines the sensor and the fuel cell characteristics. Hence, a fuel cell system can be designed that is able to detect the fuel concentration in the gas and, therefore, correct *in-situ* for fluctuations in the fuel concentration. A Ni-CZI10/$CaZr_{0.9}In_{0.1}O_{3-\alpha}$/Pt cell has been tested for this combination. Fig. 12 shows the I-V characteristics and power output of this cell at 800 °C and 5 vol.% CO_2, using 50 and 95 vol.% CH_4, respectively. The maximum power output obtained with this fuel cell system is 0.01 $mW \cdot cm^{-2}$. It is obvious that this is far too low for practical application of this system as a fuel cell. The obtained power output is also two orders of magnitude smaller than that of the first one-chamber fuel cell as reported by Iwahara *et al.* [1]. There are three possible explanations for the small power output:

(i) A relatively thick electrolyte of about 1 mm that has been used in this system. Several authors have shown that the voltage drop during the discharge of a one-chamber fuel cell based on a proton conducting electrolyte results mainly from the ohmic resistance of the electrolyte [1–4]. Hence, an increase in power output is expected when a thinner electrolyte is employed. One of the techniques that could be used to create a thin electrolyte layer is Electrostatic Spray Deposition (ESD). It has been shown that it is possible to apply ESD to produce thin layers of $BaCeO_3$ [44]. This technique has also been applied to the production of a one-chamber fuel cell based on YSZ [45].

(ii) The use of the CO_2-reforming of methane (1) instead of the partial oxidation of methane.

$$CH_4 + CO_2 \longleftrightarrow 2H_2 + 2CO$$
$$-\Delta G^0_{1073} = 28\ \text{kJ} \cdot \text{mol}^{-1} \quad (1)$$

$$CH_4 + \frac{1}{2}O_2 \longleftrightarrow 2H_2 + CO$$
$$-\Delta G^0_{1073} = 218\ \text{kJ} \cdot \text{mol}^{-1} \quad (4)$$

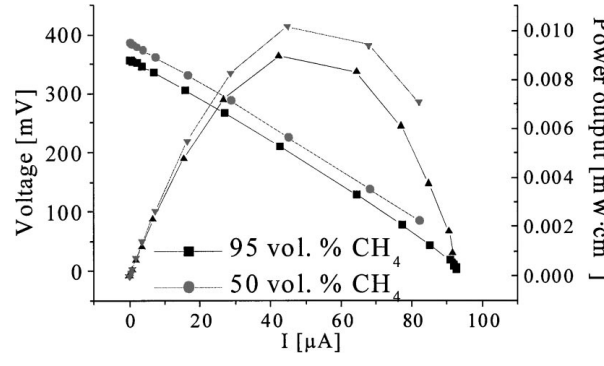

Figure 12 Characteristics and power output of the Ni-CZI10/$CaZr_{0.9}InO_{3-\alpha}$/Pt cell at 800 °C, 5 vol.% CO_2 and 50 vol.% and 95 vol.% CH_4, respectively.

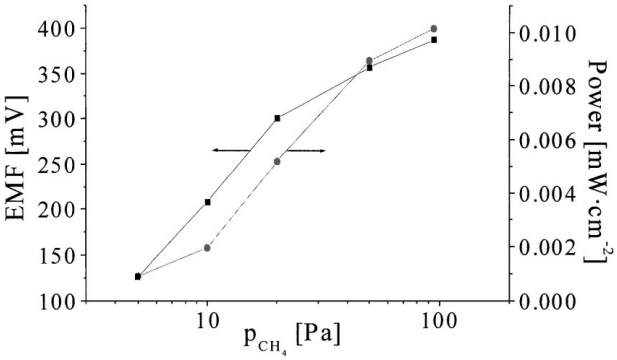

Figure 13 Power output as a function of the methane partial pressure and sensor response of the Ni-CZI10/$CaZr_{0.9}InO_{3-\alpha}$/Pt cell at 800 °C and 5 vol.% CO_2.

The calculated ΔG of the partial oxidation shows that this reaction is energetically favourable to the reforming reaction [14]. Since the potential of the cell is directly related to the ΔG of the reaction [8], the use of reaction (1) leads to a lower power output with respect to a fuel cell using the partial oxidation of methane.

(iii) The electrode materials chosen. As discussed before, in the case of a one-chamber fuel cell it is not necessary for the counter electrode to show catalytic activity. Hence, a maximum catalytic activity difference between the two electrodes can be selected. In the sensor system this is not possible, because the potential difference is not defined if the counter electrode is inactive. Because the power output is related to the difference in catalytic activity between the electrodes, a lower power density is expected with decreasing catalytic activity difference between the electrodes. Therefore, to be able to apply this device both as a sensor and a fuel cell, an electrode combination should be found that exhibits a maximum difference in catalytic activity, but where the counter electrode is still active enough to ensure a sensor response.

Fig. 13 shows the combined fuel cell and sensor characteristics at 800 °C of the Ni-CZI10/CZI10/Pt cell. This figure shows a linear dependence of the EMF on the methane partial pressure. Hence, methane detection using this cell is possible while at the same time electrical power output can be obtained. However, as discussed before, further optimisation is required in order to create a sufficient power density.

4. Conclusions

Based on the different catalytic properties of two electrodes a catalytic methane sensor has been developed. The stability of the sensor depends strongly on the electrolyte material chosen. The high-temperature perovskite proton conductor $SrCe_{0.95}Yb_{0.05}O_{3-\alpha}$ is shown to be chemically instable in CO_2 and CH_4 containing ambients. Due to this electrolyte instability the sensor stability of a Ru/$SrCe_{0.95}Yb_{0.05}O_{3-\alpha}$/Pt cell is found to be in the order of only one day. Another high-temperature perovskite proton conductor, i.e. $CaZr_{0.9}In_{0.1}O_{3-\alpha}$ (CZI10) has been found to be stable in CO_2 and CH_4 containing atmospheres. Application of this electrolyte is shown to increase the long-term stability of the sensor. The long-term stability of the sensor is further increased by a newly developed Ni-CERMET electrode based on CZI10. The long-term stability of a resulting Ni-CZI10/$CaZr_{0.9}In_{0.1}O_{3-\alpha}$/Pt sensor is found to be at least 40 days. A linear dependence of the EMF on the applied methane partial pressure is found for both the Ru/$SrCe_{0.95}Yb_{0.05}O_{3-\alpha}$/Pt and the CZI10/$CaZr_{0.9}In_{0.1}O_{3-\alpha}$/Pt sensors at 500 °C and 600 °C, respectively. Deviations from this linear behaviour can be explained by the temperature dependence of the catalytic activity of the electrode materials used.

Because the sensor principle is based on the one-chamber fuel cell design, the power output of a Ni-CZI10/$CaZr_{0.9}In_{0.1}O_{3-\alpha}$/Pt cell is also determined. The maximum power output of this system is 0.01 $mW \cdot cm^{-2}$. This low power output is caused by (a) the relatively thick electrolyte (1 mm), (b) the use of the CO_2-reforming of methane instead of the partial oxidation reaction, and (c) the employed electrode materials. In order to obtain an electrochemical device that combines both electrical power and methane detection different electrode materials should be chosen. The electrode materials that are required must have a catalytic activity difference that is large, while the counter electrode should still exhibit a high enough catalytic activity to establish a methane partial pressure dependent EMF.

References

1. T. HIBINO and H. IWAHARA, *Chem. Lett.* (1993) 1131.
2. T. HIBINO, K. ASANO and H. IWAHARA, *ibid.* (1994) 485.
3. K. ASANO, T. HIBINO and H. IWAHARA, *SOFC-IV* **95-1** (1995) 58.
4. K. ASANO, T. HIBINO and H. IWAHARA, *J. Electrochem. Soc.* **142** (1995) 3241.
5. T. HIBINO, S. WANG, S. KAKIMOTO and M. SANO, *Solid State Ionics* **127** (2000) 89.
6. *Idem., Electrochem. Solid-State Lett.* **2** (1999) 317.
7. T. HIBINO, Y. KUWAHARA and S. WANG, *J. Electrochem. Soc.* **146** (1999) 2821.
8. I. RIESS, P. J. v. d. PUT and J. SCHOONMAN, *Solid State Ionics* **82** (1995) 1.
9. M. J. G. JAK, S. RAZ, L. N. v. RIJ and I. RIESS, *Solid State Ionics*, submitted.
10. J. LE, L. N. v. RIJ and J. SCHOONMAN, *J. Electrochem. Soc.*, accepted for publication (2000).
11. L. N. VAN RIJ, R. C. VAN LANDSCHOOT and J. SCHOONMAN, in Proc. 11th Eur. Conf. Solid State Transducers, Eurosensors XI (1997) Vol. 1, p. 143.
12. L. N. v. RIJ, R. VAN LANDSCHOOT and J. SCHOONMAN, in Proc. 12th International Conference on Solid State Ionics, Halkidiki, Greece, 1999, p. 574.
13. J. R. ROSTRUP-NIELSEN and J. H. B. HANSEN, *J. Catal.* **144** (1993) 38.
14. P. D. F. VERNON, M. L. H. GREEN, A. K. CHEETHAM and A. T. ASHCROFT, *Cat. Today* **13** (1992) 417.
15. D. QIN and J. LAPSZEWICZ, *ibid.* **21** (1994) 551.
16. H. IWAHARA, T. ESAKA, H. UCHIDA and N. MAEDA, *Solid State Ionics* **3/4** (1981) 359.
17. H. IWAHARA, H. UCHIDA and N. MAEDA, *J. Power Sources* **7** (1982) 293.
18. *Idem., Solid State Ionics* **11** (1983) 109.
19. H. UCHIDA, H. YOSHIKAWA and H. IWAHARA, *ibid.* **34** (1989) 103.
20. H. UCHIDA, N. MAEDA and H. IWAHARA, *ibid.* **11** (1983) 117.

21. T. SCHERBAN and A. S. NOWICK, *ibid.* **35** (1989) 189.
22. H. IWAHARA, H. UCHIDA, K. MORIMOTO and S. HOSOGI, *J. Appl. Electrochem.* **19** (1989) 448.
23. H. UCHIDA, S. TANAKA and H. IWAHARA, *J. Appl. Electrochem.* **15** (1985) 93.
24. H. MATSUMOTO, Y. IIDA and H. IWAHARA, *ibid.* **127** (2000) 345.
25. H. MATSUMOTO, T. SUZUKI and H. IWAHARA, *ibid.* **116** (1999) 99.
26. G. MARNELLOS, O. SANOPOULOU, A. RIZOU and M. STOUKIDES, *ibid.* **97** (1997) 375.
27. F. DESCHUTTER, J. VANGRUNDERBEEK, J. LUYTEN and W. ENGELEN, *Sensors and Actuators B* **24/25** (1995) 462.
28. M. H. ZHENG and X. X. ZHEN, *Metall. Trans. B* **24** (1993) 789.
29. H. IWAHARA, *Solid State Ionics* **77** (1995) 289.
30. *Idem., ibid.* **86–88** (1996) 9.
31. *Idem., Solid State Ionics: Materials and Applications* (1992) 247.
32. T. YAJIMA, H. KAZEOKA and H. IWAHARA, *Solid State Ionics* **47** (1991) 271.
33. H. IWAHARA, T. YAJIMA, T. HIBINO, K. OZAKI and H. SUZUKI, *ibid.* **61** (1993) 65.
34. K. D. KREUER, *ibid.* **97** (1997) 1.
35. S. V. BHIDE and A. V. VIRKAR, *J. Electrochem. Soc.* **146** (1999) 2038.
36. M. J. SCHOLTEN, J. SCHOONMAN, J. C. V. MILTENBURG and H. A. J. OONK, *Solid State Ionics* **61** (1993) 83.
37. N. KURITA, N. FUKATSU and T. OHASHI, *J. Jpn. Inst. Met.* **58** (1994) 782.
38. W. ENGELEN, A. BUEKENHOUDT, J. LUYTEN and F. DESCHUTTER, *Solid State Ionics* **96** (1997) 55.
39. T. YAJIMA, K. KOIDE, N. FUKATSU, T. OHASHI and H. IWAHARA, *Sensors and Actuators B* **13/14** (1993) 697.
40. H. IWAHARA, H. UCHIDA and S. TANAKA, *J. Appl. Electrochem.* **16** (1986) 663.
41. H. IWAHARA, T. ESAKA, H. UCHIDA and K. GAKI, *Solid State Ionics* **18/19** (1986) 1003.
42. J. LE, L. N. VAN RIJ, R. C. VAN LANDSCHOOT and J. SCHOONMAN, *J. Eur. Cer. Soc.* **19** (1999) 2589.
43. L. N. VAN RIJ, L. WINNUBST, J. LE and J. SCHOONMAN, *J. Mat. Chem.* **10**(11) (2000) 2515.
44. E. M. KELDER, O. C. J. NIJS and J. SCHOONMAN, *Solid State Ionics* **68** (1994) 5.
45. N. L. H. STELZER, C. H. CHEN, L. N. V. RIJ and J. SCHOONMAN, in 10th IEA SOFC Workshop, Annex VII, Les Diablerets, Zwitserland, 1997, Vol. 2, p. 236.

Received 4 May
and accepted 14 June 2000